Progress In Electromagnetics Research M, Vol. 32, 145–155, 2013

TIME-REVERSAL FOCUS-GAIN FLATNESS OF POLARIZATION-VARYING ELECTROMAGNETIC FIELDS IN RECTANGULAR RESONANT CAVITY

Yingming Chen[1, 2], Bing-Zhong Wang[1, *], and Hong-Cheng Zhou[1]

[1]Institute of Applied Physics, University of Electronic Science and Technology of China, Chengdu 610054, China

[2]School of Physics and Electronic Information, Huaibei Normal University, Huaibei 235000, China

Abstract—In this work, theoretical analysis and numerical results are given for time-reversal (TR) focus gains of polarization-varying electromagnetic fields in a rectangular resonant cavity. To demonstrate the gains in different polarization states of the static transceivers and the ones of the rotatable transceivers, the 3 dB attenuation areas of TR angle gain (AG) and AG flatness are first calculated. The flat area is about equivalent to the range of two centrosymmetric octants in a three-dimensional Cartesian coordinate. Phase-frequency waterfalls verify the polarization-rotational rheology of the TR focus gain, in which uniform and smooth areas will contribute higher gain than uneven and rough areas.

1. INTRODUCTION

Due to spatial polarization, electromagnetic (EM) fields will differ from scalar fields. When time and space symmetries of EM fields are discussed, their vector characteristics will play a complex role because material EM properties and boundary geometry must be involved in the process of establishing EM polarization [1]. Researches on the EM polarization will concern two basic purposes at least. One is to explore further applications of EM vector characteristics in the case of combining some novel EM technologies. The other is to analyze the polarization-varying stability of a time-varying EM

Received 27 May 2013, Accepted 29 July 2013, Scheduled 31 July 2013

* Corresponding author: Bing-Zhong Wang (bzwang@uestc.edu.cn).

system. Time-reversal (TR) EM technology [2] has shown some absorbing novelties, such as far-field TR focusing beyond the diffraction limit [3, 4], TR subwavelength imaging [5], high TR focus gain in dense multipath environments [6, 7], TR-MUSIC algorithm for small scatterer localization [8], TR ultra wideband communications [4, 6, 9–11], and TR method for arbitrarily structured beam-steering arrays [12]. Mechanical motions of EM transceivers can be resolved into rotation and translation. The rotation will result in the polarization varying, which is one of our research backgrounds.

The other application background comes from widely-used enclosed cavities such as reverberation chambers, tunnels, containers, ship's compartments, missile silos, and computer chassis. Particularly, TR EM technology has also been introduced into ultra wideband wireless communication in metallic box [13], wireless sensor network in chamber environment [14], detection of small objects in reverberant cavity [15], target detection in a metal pipe [16], and efficiency measurement of ultra wideband antenna in reverberation chambers [17]. Physically, enclosed cavities will show significant multipath effects which will result in high TR focus gains [6, 7, 13–17], and the geometry of enclosed cavities in the presence of some spatial symmetries will affect the spatial patterns of TR EM focus. In addition, the boundaries of conductor cavities will restrict the EM polarizations. Consequently, this paper will focus on the TR focus gains of the polarization-varying EM fields in a rectangular resonant cavity, where two points will be researched: TR focus gains in the different polarization states of the static transceivers and the ones of the rotating transceivers.

2. THEORETICAL PREPARATION

We employ the tensor function $\overline{\overline{\mathbf{G}}}(\mathbf{r}_R|\mathbf{r}_T;t)$ to help establish the signal transmitting response $s(\mathbf{r}_R|\mathbf{r}_T;t)$ in time domain between the transmitting end at $\mathbf{r}_T$ and the receiving end at $\mathbf{r}_R$.

$$s\left(\mathbf{r}_R|\,\mathbf{r}_T;t\right)=\left[\mathbf{P^T}\left(\mathbf{r}_R,t\right)\cdot\overline{\overline{\mathbf{G}}}\left(\mathbf{r}_R|\,\mathbf{r}_T;t\right)\cdot\mathbf{P}\left(\mathbf{r}_T,t\right)\right]\otimes s\left(\mathbf{r}_T,t\right). \quad (1)$$

where $\otimes$ is the convolution and $s(\mathbf{r}_T,t)$ the signal to be transmitted. Two vectors $\mathbf{P}(\mathbf{r}_T,t)$ and $\mathbf{P}(\mathbf{r}_R,t)$ represent the polarization directions of the transmitting end and the receiving end respectively, and satisfy

$$\mathbf{P^T}\left(\mathbf{r}_T,t\right)\cdot\mathbf{P}\left(\mathbf{r}_T,t\right)=\mathbf{P^T}\left(\mathbf{r}_R,t\right)\cdot\mathbf{P}\left(\mathbf{r}_R,t\right)=1. \quad (2)$$

In a rectangular resonant cavity, the tensor $\overline{\overline{\mathbf{G}}}(\mathbf{r}_R|\mathbf{r}_T;t)$ can be obtained by numerical simulations or theoretical derivation from image method.

$$\overline{\overline{\mathbf{G}}}\left(\mathbf{r}_R|\,\mathbf{r}_T;t\right) = \begin{bmatrix} G_{xx}\left(\mathbf{r}_R|\,\mathbf{r}_T;t\right) & G_{xy}\left(\mathbf{r}_R|\,\mathbf{r}_T;t\right) & G_{xz}\left(\mathbf{r}_R|\,\mathbf{r}_T;t\right) \\ G_{yx}\left(\mathbf{r}_R|\,\mathbf{r}_T;t\right) & G_{yy}\left(\mathbf{r}_R|\,\mathbf{r}_T;t\right) & G_{yz}\left(\mathbf{r}_R|\,\mathbf{r}_T;t\right) \\ G_{zx}\left(\mathbf{r}_R|\,\mathbf{r}_T;t\right) & G_{zy}\left(\mathbf{r}_R|\,\mathbf{r}_T;t\right) & G_{zz}\left(\mathbf{r}_R|\,\mathbf{r}_T;t\right) \end{bmatrix}$$

$$= \left[\overline{\overline{\mathbf{G}}}\left(\mathbf{r}_T|\,\mathbf{r}_R;t\right)\right]^{\mathbf{T}} = \begin{bmatrix} \mathbf{G}_x\left(\mathbf{r}_T|\,\mathbf{r}_R;t\right) \\ \mathbf{G}_y\left(\mathbf{r}_T|\,\mathbf{r}_R;t\right) \\ \mathbf{G}_z\left(\mathbf{r}_T|\,\mathbf{r}_R;t\right) \end{bmatrix}. \tag{3}$$

Through three transient simulations in Microwave CST studio, we can get $\mathbf{G}_x(\mathbf{r}_T|\mathbf{r}_R;t)$, $\mathbf{G}_y(\mathbf{r}_T|\mathbf{r}_R;t)$, and $\mathbf{G}_z(\mathbf{r}_T|\mathbf{r}_R;t)$, respectively. Or, by using image method, we can also get their expressions in the multipath form of infinite series.

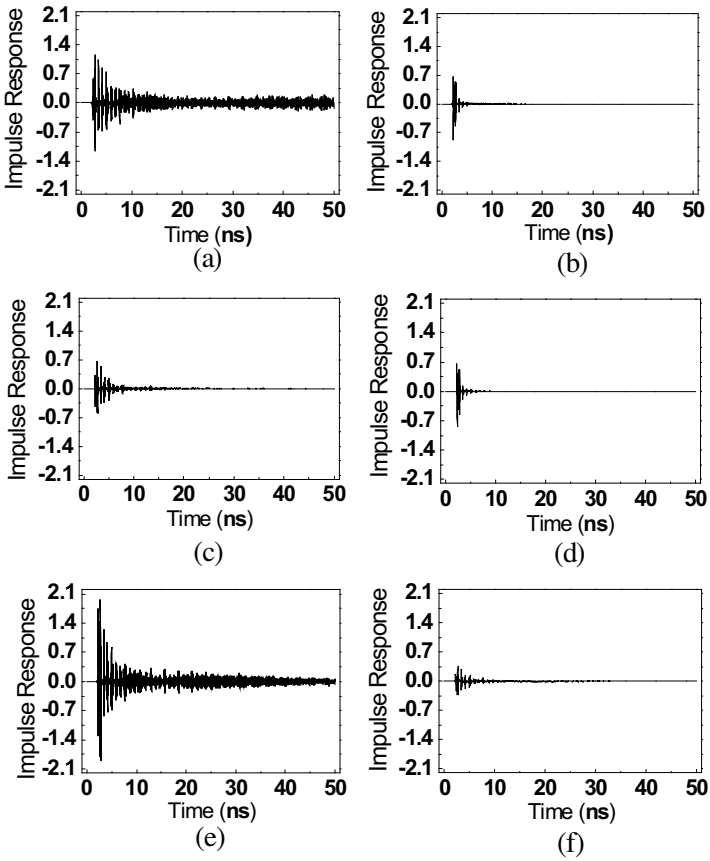

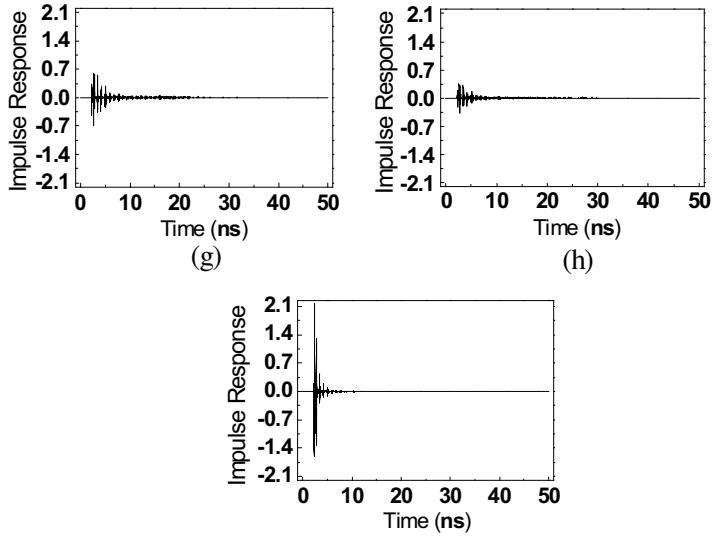

Figure 1. Nine components of the tensor $\overline{\overline{\mathbf{G}}}(\mathbf{r}_R|\mathbf{r}_T;t) \otimes s(\mathbf{r}_T,t)$, where (a), (b) and (c) are the three components of the vector $\mathbf{G}_x(\mathbf{r}_T|\mathbf{r}_R;t) \otimes s(\mathbf{r}_T,t)$, the middle three (d), (e) and (f) are the three ones of $\mathbf{G}_y(\mathbf{r}_T|\mathbf{r}_R;t) \otimes s(\mathbf{r}_T,t)$, the last three (g), (h) and (i) are the three ones of $\mathbf{G}_z(\mathbf{r}_T|\mathbf{r}_R;t) \otimes s(\mathbf{r}_T,t)$.

From the viewpoint of Expression (1), the temporal variability of the system will be totally reflected in $\overline{\overline{\mathbf{G}}}(\mathbf{r}_R|\mathbf{r}_T;t)$, $\mathbf{P}(\mathbf{r}_T,t)$, and $\mathbf{P}(\mathbf{r}_R,t)$, which depend explicitly on the time variable. The variability of the environments will be reflected in $\overline{\overline{\mathbf{G}}}(\mathbf{r}_R|\mathbf{r}_T;t)$, and the polarization varying will be partially reflected in $\mathbf{P}(\mathbf{r}_T,t)$ and $\mathbf{P}(\mathbf{r}_R,t)$. Considering the constraints of Expression (2), we can introduce angle parameters $\mathbf{\Phi}_T$: (θ_T,φ_T) and $\mathbf{\Phi}_R$: (θ_R,φ_R), then

$$\begin{aligned}
\mathbf{P}\left(\mathbf{r}_T,t\right) &= \begin{bmatrix} \sin\theta_T\cos\varphi_T \\ \sin\theta_T\sin\varphi_T \\ \cos\theta_T \end{bmatrix} = \mathbf{P}\left(\mathbf{r}_T,\mathbf{\Phi}_T\right), \\
\mathbf{P}\left(\mathbf{r}_R,t\right) &= \begin{bmatrix} \sin\theta_R\cos\varphi_R \\ \sin\theta_R\sin\varphi_R \\ \cos\theta_R \end{bmatrix} = \mathbf{P}\left(\mathbf{r}_R,\mathbf{\Phi}_R\right). \qquad (4)
\end{aligned}$$

Through Expression (4), we map the polarization varying to the state space $\mathbf{\Phi}$: $(\mathbf{\Phi}_R;\mathbf{\Phi}_T)$ consisting of four angle parameters. It is obvious that the state space can completely describe the polarization

variability. Any real rotation of the polarizations can be projected onto a continuous streamline in $\mathbf{\Phi}$ space, and in turn, any streamline in $\mathbf{\Phi}$ space may represent a possible rotation. In this way, the polarization-varying gain analysis can be transformed into the angle gain (AG) analysis and AG flatness (AGF) analysis. We define the TR focus AG (AG^{TR}) and AGF (AGF^{TR}) as follows.

$$\mathrm{AG}^{TR}\left(\mathbf{r}_T, \mathbf{r}_R; \mathbf{\Phi}', \mathbf{\Phi}\right) = 10\mathbf{log}\frac{s^{TR}\left(\mathbf{r}_T, \mathbf{r}_R; \mathbf{\Phi}, \mathbf{\Phi}\right)}{s^{TR}\left(\mathbf{r}_T, \mathbf{r}_R; \mathbf{\Phi}', \mathbf{\Phi}'\right)}. \tag{5}$$

$$\mathrm{AGF}^{TR}\left(\mathbf{r}_T, \mathbf{r}_R; \mathbf{\Phi}', \mathbf{\Phi}\right) = 10\mathbf{log}\frac{s^{TR}\left(\mathbf{r}_T, \mathbf{r}_R; \mathbf{\Phi}', \mathbf{\Phi}\right)}{s^{TR}\left(\mathbf{r}_T, \mathbf{r}_R; \mathbf{\Phi}', \mathbf{\Phi}'\right)}. \tag{6}$$

$$\begin{cases} s_{pulse}\left(\mathbf{r}_R|\,\mathbf{r}_T; \mathbf{\Phi}', t\right) \\ = \left[\mathbf{P^T}\left(\mathbf{r}_R, \mathbf{\Phi'}_R\right) \cdot \overline{\overline{\mathbf{G}}}\left(\mathbf{r}_R|\,\mathbf{r}_T; t\right) \cdot \mathbf{P}\left(\mathbf{r}_T, \mathbf{\Phi'}_T\right)\right] \otimes \left[\delta\left(t\right)\right] \\ s^{TR}\left(\mathbf{r}_T, \mathbf{r}_R; \mathbf{\Phi}', \mathbf{\Phi}\right) \\ = \max_t \left|s_{pulse}\left(\mathbf{r}_T|\,\mathbf{r}_R; \mathbf{\Phi}, t\right) \otimes s_{pulse}\left(\mathbf{r}_R|\,\mathbf{r}_T; \mathbf{\Phi}', -t\right)\right| \end{cases}. \tag{7}$$

where $\mathbf{\Phi}'$ is a reference state, $s_{pulse}(\mathbf{r}_R|\mathbf{r}_T; \mathbf{\Phi}', t)$ the impulse response (IR) from $\mathbf{r}_T$ to $\mathbf{r}_R$ in the $\mathbf{\Phi}'$ state, and $s^{TR}(\mathbf{r}_T, \mathbf{r}_R; \mathbf{\Phi}', \mathbf{\Phi})$ the TR focus peak (carrying the TR IR of the $\mathbf{\Phi}'$ state from $\mathbf{r}_T$ back to $\mathbf{r}_R$) in the $\mathbf{\Phi}$ state. The fluctuation of AG^{TR} in $\mathbf{\Phi}$ space will show the dependence between the TR focus gains and the polarization states. The distribution of AGF^{TR} in $\mathbf{\Phi}$ space will be closely related to the polarization-varying gains. By the reciprocity in Expression (3), we can verify that AG^{TR} and AGF^{TR} are symmetrical about $\mathbf{\Phi}_T = \mathbf{\Phi}_R$ in $\mathbf{\Phi}$ space.

In many practical applications, $\mathbf{\Phi}$ space will degenerate into two dimensions, when one end of the transceivers is fixed and the other one can only rotatably scan. Then, we can draw intuitive two-dimensional contours of AG^{TR} and AGF^{TR}. Further, if the other one can only rotatably scan in single degree of freedom, we can also give phase-frequency waterfall (phase spectrum array about rotational angle) which will show the polarization-rotational rheology of the TR focus gain physically.

$$\begin{aligned} & F\left[s_{pulse}\left(\mathbf{r}_T|\,\mathbf{r}_R; \mathbf{\Phi}, t\right) \otimes s_{pulse}\left(\mathbf{r}_R|\,\mathbf{r}_T; \mathbf{\Phi}', -t\right)\right] \\ = \; & a\left(f; \mathbf{r}_T, \mathbf{r}_R; \mathbf{\Phi}', \mathbf{\Phi}\right) \exp\left[j\mathrm{Phase}\left(f; \mathbf{r}_T, \mathbf{r}_R; \mathbf{\Phi}', \mathbf{\Phi}\right)\right]. \end{aligned} \tag{8}$$

where $F[\ldots]$ represents the Fourier transform, f is the frequency, $a(f; \mathbf{r}_T, \mathbf{r}_R; \mathbf{\Phi}', \mathbf{\Phi})$ is the amplitude, and $\mathrm{Phase}(f; \mathbf{r}_T, \mathbf{r}_R; \mathbf{\Phi}', \mathbf{\Phi})$ is the phase. If $\mathbf{\Phi}' = \mathbf{\Phi}$, we can verify

$$\frac{\partial}{\partial f}\mathrm{Phase}\left(f; \mathbf{r}_T, \mathbf{r}_R; \mathbf{\Phi}', \mathbf{\Phi}\right)\Big|_{\mathbf{\Phi}'=\mathbf{\Phi}} = 0. \tag{9}$$

Expression (9) shows the inter-relation between time reversal in time domain and phase conjugation in frequency domain, which is the complete compensation of the dispersion in the whole open interval of the signal bandwidth. Therefore, if the dispersion compensation is disturbed by polarization-varying states, TR focus AG will be reduced physically.

3. CALCULATION RESULTS

The size of the ideal resonant cavity is (70 cm × 50 cm × 40 cm). The coordinate origin is located at the center of the cavity, and three axes are perpendicular to the inner surfaces of the cavity. The transmit-receive coordinates are $\mathbf{r}_T$: $(24, 13, 7)$ cm and $\mathbf{r}_R$: $(-19, -11, -5)$ cm. Through three transient simulations, we can get 9 components of the tensor $\overline{\overline{\mathbf{G}}}(\mathbf{r}_R|\mathbf{r}_T;t) \otimes s(\mathbf{r}_T,t)$ in Fig. 1, where the bandwidth of the impulse signal $s(\mathbf{r}_T,t)$ is $[3.1, 10.7]$ GHz. Multipath effects are

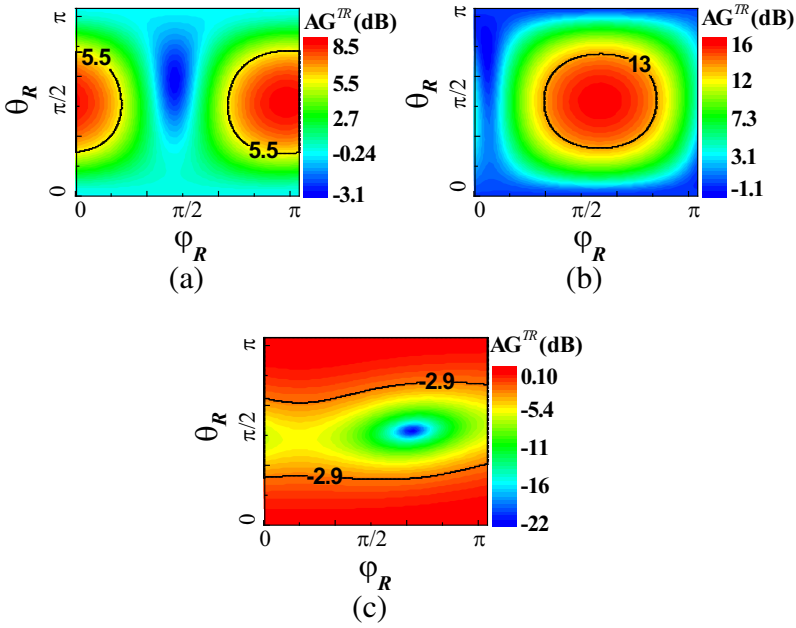

Figure 2. Three contours of AG^{TR} when $\mathbf{\Phi}_T$: $(\pi/2, 0)$, $\mathbf{\Phi}_T$: $(\pi/2, \pi/2)$, and $\mathbf{\Phi}_T$: $(0, 0)$, sequentially, in which 3 dB attenuation lines relative to the maximum gains are marked. The high-gain areas can be about more than $\pi/3 \times \pi/3$.

significant, and polarization selectivity (different polarizations will lead to different IRs) is too. Consequently, TR operation and polarization will play important roles. In addition, the reciprocity is manifested in (b) ≈ (d), (c) ≈ (g) and (f) ≈ (h) .

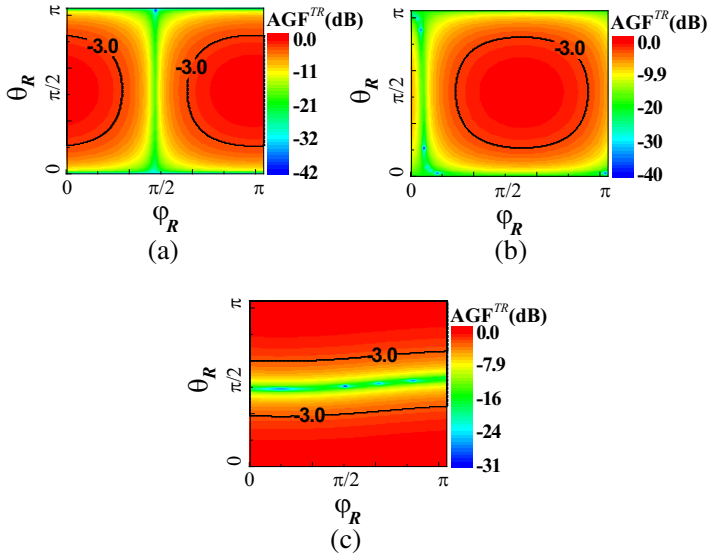

Figure 3. Three contours of AGF^{TR} with the reference state [$\mathbf{\Phi}'_T$: $(\pi/2, 0)$; $\mathbf{\Phi}'_R$: $(\pi/2, 0)$], the reference state [$\mathbf{\Phi}'_T$: $(\pi/2, \pi/2)$; $\mathbf{\Phi}'_R$: $(\pi/2, \pi/2)$], and the reference state [$\mathbf{\Phi}'_T$: $(0, 0)$; $\mathbf{\Phi}'_R$: $(0, 0)$], sequentially, in which 3 dB attenuation lines relative to the maximum gains are marked. The 3 dB stable areas can be about more than $\pi/2 \times \pi/2$.

Based on the data of Fig. 1, TR focus AG, AGF and phase-frequency waterfalls can be calculated by Digital Visual Fortran programs. We fix $\mathbf{\Phi}_T$: $(\pi/2, 0)$, $\mathbf{\Phi}_T$: $(\pi/2, \pi/2)$, and $\mathbf{\Phi}_T$: $(0, 0)$, respectively, and accordingly the contours of AG^{TR} and AGF^{TR} are shown in Fig. 2 and Fig. 3. We can intuitively read out the following three points in Fig. 2. First, for a given $\mathbf{\Phi}_T$, there are the $\mathbf{\Phi}_R$ states of the maximum and minimum gains. Second, the differences between the maximum and minimum gains can be more than 10 dB (even 20 dB). Third, the 3 dB attenuation areas are considerable (about more than $\pi/3 \times \pi/3$). Therefore, the polarization will play an important role for TR focus gains in rectangular resonant cavities. The role can be regulated by optimizing the polarizations of the transceivers, and the considerable areas of the high gain will further help to reduce the

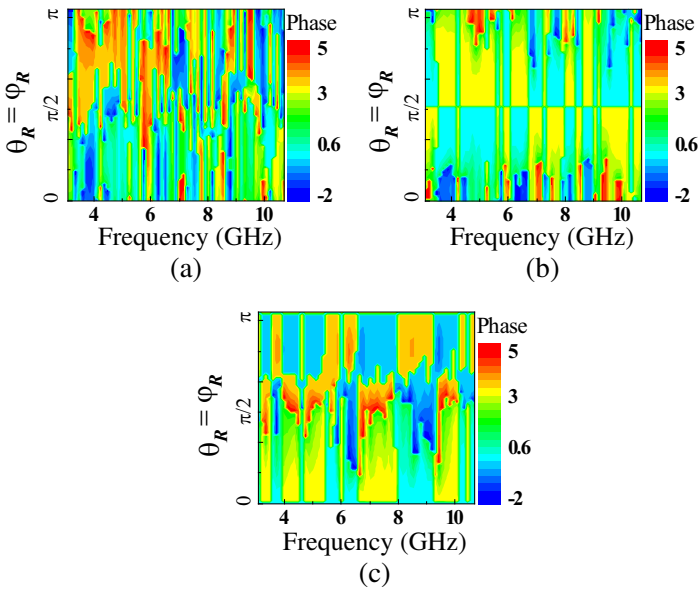

Figure 4. Three phase-frequency waterfalls down rotational angle $\theta_R = \varphi_R$ with the reference state [$\mathbf{\Phi}'_T$: $(\pi/2, 0)$; $\mathbf{\Phi}'_R$: $(\pi/2, 0)$], the reference state [$\mathbf{\Phi}'_T$: $(\pi/2, \pi/2)$; $\mathbf{\Phi}'_R$: $(\pi/2, \pi/2)$], and the reference state [$\mathbf{\Phi}'_T$: $(0, 0$; $\mathbf{\Phi}'_R$: $(0, 0)$], sequentially, where $\theta_R = \varphi_R$ represents the diagonal lines in Fig. 3.

optimization difficulty in the applications of TR communications and sensors. In addition, more than 10 dB differences of AGs in Fig. 2 will make the polarization characteristics of the targets be involved in TR EM imaging and detection. For example, if we use TR EM fields with single linear polarization to detect two targets with different polarization, the 10 dB differences will probably result in the loss of one target submerged in noises.

Figure 2 shows some references about the polarizations design of the transceivers. Fig. 3 shows AGF^{TR} when the polarization state of the receive end is rotation-variable. The 3 dB stable areas can be more than $\pi/2 \times \pi/2$. Considering the invariance of AGF^{TR} about the operation $\mathbf{\Phi}_R \to -\mathbf{\Phi}_R$, the 3 dB stable areas will be about equivalent to the ranges of two centrosymmetric octants in a three-dimensional Cartesian coordinate. The flat ranges are considerable. On the other hand, the differences between the maximum and minimum gains can be more than 30 dB (even up to 40 dB) in Fig. 3, that means steep transitions of TR focus gains. Based on the above two perspectives

(considerable flat areas and steep transition regions), Fig. 3 will imply two possible applications. One, we can use the antenna array including four to five different polarizations to balance any rotation varying without channel re-estimation. Two, we can take advantage of the steep transitions of TR focus gains to achieve high-accuracy attitude monitoring, if the rotation attitudes have been pre-set in the transition regions.

The special streamline $\theta_R = \varphi_R$ in $\mathbf{\Phi}$ space is selected which just represents the diagonal lines in Fig. 3. Then Fig. 4 shows three phase-frequency waterfalls along the diagonal line. From the physical explanation of Expressions (8) and (9), we can infer that uniform and smooth areas in the waterfalls will contribute higher TR focus gains than uneven and rough areas. The inference can also be verified by comparing the fluctuations of three AGFs along the diagonal lines in Fig. 3 and the distributions of three phases in the waterfalls of Fig. 4, respectively. There is an interesting and outstanding problem: why are the waterfalls non-continuous and clumpy?

4. CONCLUSION

This paper presents theoretical analysis and numerical results of TR focus gains of polarization-varying EM Fields in a rectangular resonant cavity, which is the first known effort to calculate the 3 dB attenuation areas of TR EM AG and AGF. The 3 dB areas of AG are about more than $\pi/3 \times \pi/3$, and the ones of AGF about more than $\pi/2 \times \pi/2$ in the case of the fixed transmit end. The flatness makes TR technology attractive for TR EM communications, imaging and detection in the case of polarization varying in enclosed cavities. More than 30 dB difference of AGF will make TR EM fields potential to develop high-accuracy rotation monitoring. Phase-frequency waterfalls intuitively show the polarization-rotational rheology of the TR focus gain, in which uniform and smooth areas will contribute higher TR focus gains than uneven and rough areas. Next works will include three issues, the translational rheology of the TR focus gains, TR detection by using EM polarization in intensive background noise, and phase-amplitude constraints of TR EM fields by Hilbert transform relation.

ACKNOWLEDGMENT

This work was supported by the National Natural Science Foundation of China (No. 61071031 and No. 61107018), the Research Fund for the Doctoral Program of Higher Education of China (No. 20100185110021 and No. 20120185130001), the Fundamental Research Funds for

the Central Universities (No. ZYGX2012YB020), and the Project ITR1113.

REFERENCES

1. Dmitriev, V., "Space-time reversal symmetry properties of electromagnetic Green's tensors for complex and bianisotropic media," *Progress In Electromagnetics Research*, Vol. 48, 145–184, 2004.
2. Lerosey, G., J. de Rosny, A. Tourin, A. Derode, G. Montaldo, and M. Fink, "Time reversal of electromagnetic waves," *Phys. Rev. Lett.*, Vol. 92, No. 19, 193904, May 2004.
3. Lerosey, G., J. de Rosny, A. Tourin, and M. Fink, "Focusing beyond the diffraction limit with far-Field time reversal," *Science*, Vol. 315, 1120–1122, Feb. 2007.
4. Ge, G.-D., D. Wang, and B.-Z. Wang, "Subwavelength array of planar triangle monopoles with cross slots based on far-field time reversal," *Progress In Electromagnetics Research*, Vol. 114, 429–441, 2011.
5. Davy, M., J.-G. Minonzio, J. de Rosny, C. Prada, and M. Fink, "Influence of noise on subwavelength imaging of two close scatterers using time reversal method: Theory and experiments," *Progress In Electromagnetics Research*, Vol. 98, 333–358, 2009.
6. Naqvi, I. H., S. A. Aleem, O. Usman, S. B. Ali, P. Besnier, and G. El. Zein, "Robustness of a time-reversal ultra-wideband system in non-stationary channel environments," *Wireless Communications and Networking Conference: PHY and Fundamentals*, 37–41, 2012.
7. Zhu, X., Z. Zhao, W. Yang, Y. Zhang, Z.-P. Nie, and Q. H. Liu, "Iterative time-reversal mirror method for imaging the buried object beneath rough ground surface," *Progress In Electromagnetics Research*, Vol. 117, 19–33, 2011.
8. Solimene, R., A. Dell'Aversano, and G. Leone, "Interferometric time reversal music for small scatterer localization," *Progress In Electromagnetics Research*, Vol. 131, 243–258, 2012.
9. Qiu, R. C., C. Zhou, N. Guo, and J. Q. Zhang, "Time reversal with MISO for ultra-wideband communications: Experimental results," *IEEE Antenna and Wireless Propagation Letters*, Vol. 5, No. 1, 269–273, 2006.
10. Guo, N., B. M. Sadler, and R. C. Qiu, "Reduced-complexity UWB time-reversal techniques and experimental results," *IEEE Trans. Wireless Comm.*, Vol. 6, No. 12, 4221–4226, Dec. 2007.

11. Zhou, C., N. Guo, and R. C. Qiu, "Time reversed ultra-wideband (UWB) multiple-input multiple-output (MIMO) based on measured spatial channels," *IEEE Trans. Vehicular Technology*, Vol. 58, No. 6, 2884–2898, Jul. 2009.
12. Zhao, D. S., Y. W. Jin, B.-Z. Wang, and R. Zang, "Time reversal based broadband synthesis method for arbitrarily structured beam-steering arrays," *IEEE Trans. Antennas Propag.*, Vol. 60, No. 1, 164–173, Jan. 2012.
13. Zhai, H., S. Jung, and M. Lu, "Wireless communication in boxes with metallic enclosure based on time-reversal ultra-wideband technique: A full-wave numerical study," *Progress In Electromagnetics Research*, Vol. 101, 63–74, 2010.
14. Li, D., J. S. Hong, and B.-Z. Wang, "Improving anti-detection/interception performance for wireless sensor network based on time-reversal technology," *The 5th International Conference on Wireless Communications, Networking and Mobile Computing (WiCom)*, 1–4, 2009.
15. Sundaralingam, P., V. Fusco, D. Zelenchuk, and R. Appleby, "Detection of an object in a reverberant environment using direct and differential time reversal," *The 6th European Conference on Antennas and Propagation (EUCAP)*, 1115–1117, 2011.
16. Moura, J. M. F. and Y. W. Jin, "Detection by time reversal: Single antenna," *IEEE Trans. Signal Process.,* Vol. 55, No. 1, 187–201, Jan. 2007.
17. Le Fur, G., P. Besnier, and A. Sharaiha, "Efficiency measurement of UWB antennas using time reversal in reverberation chambers," *Electronics Letters*, Vol. 44, No. 17, 1002–1003, Aug. 14, 2008.